

Research Article

Open-Circuit Fault Analysis and Recognition in Three-Level Inverters Based on Recurrence Plot and Convolution Neural Network

Jianjun Yan ^{1,2}, Yanxing Huang ², Shuai Yuan ², Yufan Lu ² and Zeyu Yu ²

¹Shanghai Key Laboratory of Intelligent Sensing and Detection Technology, East China University of Science and Technology, Shanghai 200237, China

²School of Mechanical and Power Engineering, East China University of Science and Technology, Shanghai 200237, China

Correspondence should be addressed to Jianjun Yan; jjyan@ecust.edu.cn

Received 11 January 2023; Revised 18 June 2023; Accepted 8 September 2023; Published 3 October 2023

Academic Editor: C. Dhanamjayulu

Copyright © 2023 Jianjun Yan et al. This is an open access article distributed under the Creative Commons Attribution License, which permits unrestricted use, distribution, and reproduction in any medium, provided the original work is properly cited.

Power electronics is vital to modern infrastructure, but it is susceptible to open-circuit faults that can cause serious damage. Three-level inverters are commonly used in such equipment, but their high sensitivity and probability of failure make them particularly challenging to diagnose. In this groundbreaking study, we present a new method for accurately detecting and locating open-circuit faults in three-level, neutral-clamped inverters. Using advanced simulation tools and nonlinear dynamic methods, we develop a new diagnostic model that outperforms existing fault classification algorithms. By converting the current signal into an unthreshold recurrence plot (URP) and mapping its nonlinear features to a two-dimensional plane, it is possible to extract key spatial information and train a residual neural network model for fault diagnosis. The method represents a major advance in power electronics and has the potential to save equipment from costly damage. By accurately detecting and locating open-circuit faults in three-level inverters, the reliability and safety of power electronics can be guaranteed for years to come.

1. Introduction

As the key component responsible for converting direct current (DC) into alternating current (AC) signals, inverters have been widely used in converter systems. Because of their low total standing voltage, low total harmonic distortion, and ability to reduce electromagnetic interference effectively, multilevel inverters have been regarded as one of the most preferable circuit configurations for high-efficiency DC-AC links [1]. Numerous multilevel inverters have been developed, such as neutral-point-clamped (NPC) [2], flying capacitor [3], and cascaded H-bridge (CHB) multilevel inverters [4]. Because of their low output harmonic distortion and load impact, neutral-point-clamped three-level inverters have been widely used in flexible AC transmission technologies, such as in static synchronous compensators, active power filters, large motor drivers, and wind power generators, which

involve medium- and high-voltage frequency conversion. Insulated gate bipolar transistors (IGBTs) have been used as power switches in inverters, which can be switched on for an extended period of time under high-pressure, high-temperature, and high-frequency conditions [5]. Compared with two-level inverters, three-level inverters have a higher number of power switches and thus more complex circuits and higher instability [6]. Short- or open-circuit failures are regarded as the most common type of power switch failure in inverters [7]. When a short-circuit fault occurs in an IGBT, the local current considerably increases. To rectify this problem, an inverter is used to achieve self-protection. When an IGBT exhibits an open-circuit fault, the IGBT is in the off state. Failure to locate a fault accurately in time results in considerable damage to an inverter [8]. Because open-circuit faults cannot be detected by standard protection systems, the present study focused on open-circuit faults.

Because diagnosing open-circuit faults is critical in inverters [9, 10], numerous fault diagnosis methods have been proposed. These methods can be divided into voltage- and current-based methods. In voltage-based methods, diagnosis is achieved by examining the difference between the fault voltage and the normal reference voltage. For example, in [11], a fault diagnosis method based on zero-voltage vector sampling and three-phase current reconstruction was proposed. In [12], a multiscale adaptive fault diagnosis method based on symmetric signal reconstruction preprocessing was proposed to diagnose arbitrary switching faults of microgrid inverters under variable load conditions. In [13], an open-circuit fault diagnosis technology was proposed for a five-level CHB multilevel inverter switch device based on fuzzy logic control. In [14], an analytical model based on the difference between fault-state instantaneous voltage and measured signals was proposed. However, the aforementioned voltage-based methods require additional voltage sensors and complex analysis units and are easily influenced by load changes.

Current-based, open-circuit fault diagnosis methods based on the output current change trend and direction of power switches are commonly used in inverters [15]. In these methods, Park's transform techniques are commonly adopted. For example, in [16], a fault diagnosis method based on the vector current and instantaneous average angle was proposed. In [17], an open-circuit fault diagnosis method based on rotor current variations was proposed. In [18], a residual-based current method was proposed to diagnose converter faults through comparison with an adaptive threshold. In [19], a three-phase reference current error method was used to detect open-circuit faults in an inverter. In general, diagnostic variables are calculated using the average of three-phase reference current errors, and a fast converter is obtained through comparison with a defined threshold. However, although the calculation cost is low, the threshold can be difficult to determine, especially when the load changes.

At present, numerous algorithms based on signal and knowledge methods have demonstrated high performance in inverter fault diagnosis [20]. For example, in [21], a two-step diagnosis method based on artificial neural networks (NNs) was proposed to identify multiple open-circuit faults in three-phase converters. In [22], a fault diagnosis method based on principal component analysis and support vector machines (SVMs) was proposed for cascading multilevel inverters. In [23], a low-frequency sampling method was developed to classify the main fault components and NNs for fault diagnosis in inverters. In [24], a novel convolutional NN was proposed for rapid fault diagnosis in DC-DC inverters. In [25], a wavelet decomposition method for fault current signal processing and an SVM online fault diagnosis model for classification were proposed. In [26], a fault detection and diagnosis method for three-phase inverters based on NNs was proposed. In [27], a diagnostic technique based on discrete wavelet transform and NNs was proposed. In [28], fast Fourier transform (FFT) was used to extract features and an SVM was used to classify the faults of multilevel inverters. In [29], a fault feature extraction

method based on joint eigenmatrix approximate diagonalisation and independent component analysis (JADE-ICA) was proposed and an NN was used as a fault classification method. This JADE-ICA algorithm can effectively make both the source signal and the separated signal correspond one to one and overcome the influence of nonlinear time differences. In [30], an adaptive electrical period partition (AEPP) algorithm was designed to pick single electrical periods from real-time three-phase current signals. Feature analysis and normalization of electrical period signals were performed based on maximal overlap discrete wavelet transformation (MODWT) and Park's vector modulus (PVM). Random forest was utilized to construct the fault diagnosis model with the high accuracy of fault identification.

Because of the complex nonlinear relationship between the fault types and fault characteristics of voltage or current signals reported in previous studies on inverter open-circuit faults, defining an optimal feature set to differentiate between the various types of faults is difficult. Therefore, a considerable amount of nonlinear information is usually lost from voltage or current signals. Recurrence plots (RPs) are an effective means for analysing the nonlinear characteristics of signals in the phase space. Compared with other nonlinear methods, RPs have lower requirements in terms of signal length and stability and are therefore highly suitable for the analysis of nonlinear dynamic systems. Compared with RPs, URPs are free from the restriction of the threshold value and thus retain more nonlinear information. In addition, convolutional NNs simulate the structure of human neurons to transmit information layer by layer and achieve automatic feature extraction. In many studies, the features extracted by convolutional NNs have been confirmed to be more representational than conventional artificial extracted features, thus allowing for improved classification and recognition. These results indicate that the proposed fault diagnosis method preserves nonlinear information between fault types and current signals, realises automatic feature extraction from current signals, and is particularly suitable for open-circuit fault diagnosis in NPC inverters.

The proposed method consists of three parts: fault signal generation, signal conversion, and model construction. In fault signal generation, a simulation model of a three-level inverter is constructed using the Simulink module of MATLAB, and the current signal waveform corresponding to one fault-free scenario and 10 open-circuit faults is calculated. For fully exploring the nonlinear features of the current signal, a nonlinear dynamic method is used to convert current signals into URPs. This step allows the nonlinear features of URPs to be mapped to a two-dimensional plane and enables the spatial features of the current signals to be retained and extracted. Finally, a ResNet50 residual NN is used to self-learn and train the features of URPs to obtain a current signal classification model for differentiating between the current signals of different fault types. The results of this study indicate that the proposed method has high recognition accuracy in inverter open-circuit fault diagnosis.

The rest of this paper is organised as follows: In Section 2, the main faults of three-level NPC inverters are described. Section 3 explains the proposed current signal analysis and recognition method based on URPs and convolutional NNs, which involves the combination of a nonlinear analysis method with deep learning. Section 4 presents the results of comparative experiments conducted to evaluate the effectiveness of the proposed fault diagnosis algorithm. Finally, Section 5 provides the conclusions of this study.

Figure 1 illustrates the overall process of the proposed method for diagnosing open-circuit faults in three-level inverters. First, the current signals corresponding to various open-circuit faults were converted into URPs. Then, a ResNet50 residual NN [31] was utilized to extract and classify the features of current signal RP. Finally, a model for identifying different open-circuit faults in three-level inverters was developed.

2. Three-Level NPC Inverter Fault Analysis

The wind turbine's wind wheel rotates due to the force of the wind, which converts the wind's kinetic energy into the mechanical energy of the wind wheel shaft. The generator is then driven by the wind wheel shaft to produce electricity. To transmit this electricity to the grid, it needs to be fully rectified and inverted by using a converter. The three-level inverter is a device that converts direct current (DC) to alternating current (AC) and is mainly used as the rotor (motor) side of the wind turbine converter system. It is considered a core component of the converter.

In this study, a diode-clamped (NPC) three-level inverter is utilized. The advantage of this topology is its low switching losses and ability to control reactive power. In addition, the waveform quality of the output voltage is better due to the switching tubes' withstand voltage level being twice as high as that of a conventional two-level inverter. The diode-clamped three-level inverter is composed of three bridge arms, with each arm consisting of two clamping diodes, four power diodes, and four current-continuity diodes. Figure 2 depicts the schematic diagram of a three-level inverter.

A diode-clamped three-level inverter was used as an example for fault analysis. The inverter was mainly composed of two series DC support capacitors and A-B-C three-phase bridge arms at the DC side. Each phase bridge arm consisted of two clamping diodes, four IGBT power switches, and four freewheeling diodes. As shown in Figure 3, the Simulink module of MATLAB was used to construct a simulation model of a three-level inverter.

The primary circuit of the three-level inverter consisted of 12 IGBTs. When an open-circuit fault occurred in an IGBT, the probability of having an open circuit in one or two IGBTs increased, whereas the probability of having an open circuit in three or more IGBTs decreased. This study focused on the open-circuit faults of one or two IGBT power switches. Based on the above two faults, inverter faults were divided into six categories in this study, as presented in Table 1.

According to the classification of inverter faults, an open-circuit fault model was established using the Simulink module. In the Simulink simulation module, SS1 was created as the conduction module of switch S1. When the SS1 conduction module was connected to switch S1, the output was an SPWM pulse. When the SS1 conduction module was disconnected from switch S1, the output was a constant value of 0, which is equivalent to no pulse, simulating the open state of the IGBT tube. Because the three-bridge arms in the three-level inverter correspond to the three-phase current waveforms of A, B, and C, respectively, there is no difference in amplitude between each phase current, only phase change. Therefore, the A-phase current was used in this paper to display the output waveform of the open-circuit fault of the inverter. The typical simulation waveforms of 11 types of open-circuit fault in a three-level inverter are shown in Figure 4.

3. Research Method

3.1. URPs of Current Signals. RPs are an essential method for analysing the periodicity, chaos, and nonstationarity of time series and for examining the nonlinear dynamic characteristics of different systems. They are capable of revealing the internal structure of time series and providing preliminary data on similarity, information content, and predictability. The first step in obtaining RPs involves the phase space reconstruction of the signal. According to embedding theory, an appropriate embedding dimension m and delay time R must be selected to reconstruct the phase space. The reconstructed vector is represented as follows:

$$X_i = (x_i + x_{i+\tau} + \dots + x_{i+(m-1)\tau}), \quad i = 1, 2, \dots, N, \quad (1)$$

where $N = n - (m - 1)\tau$. The distance between any two points in the phase space is defined as follows:

$$D_{ij} = \|X_i - X_j\|, \quad i = 1, 2, \dots, N. \quad (2)$$

By selecting a suitable threshold ε , the recursive matrix can be obtained as follows:

$$R_{i,j} = \theta(\varepsilon - D_{i,j}), \quad (3)$$

where $\theta(\bullet)$ is a Heaviside function, which is expressed as follows:

$$\theta(x) = \begin{cases} 1, & x \geq 0, \\ 0, & x < 0. \end{cases} \quad (4)$$

RPs can intuitively map the motion state in the high-dimensional phase space of a signal to a two-dimensional plane, thus reflecting its nonlinear dynamic characteristics [32]. When the distance $D_{i,j}$ between X_i and X_j is less than ε , the motion states between them are highly similar. Thus, the motion states are recurrent, and the value of $R_{i,j}$ is 1, which is represented by a black dot in the figure. By contrast, when the distance $D_{i,j}$ between X_i and X_j is greater than ε , the motion states between them are extremely different. Thus, the value of $R_{i,j}$ is 0, which is represented by a white dot in the figure.

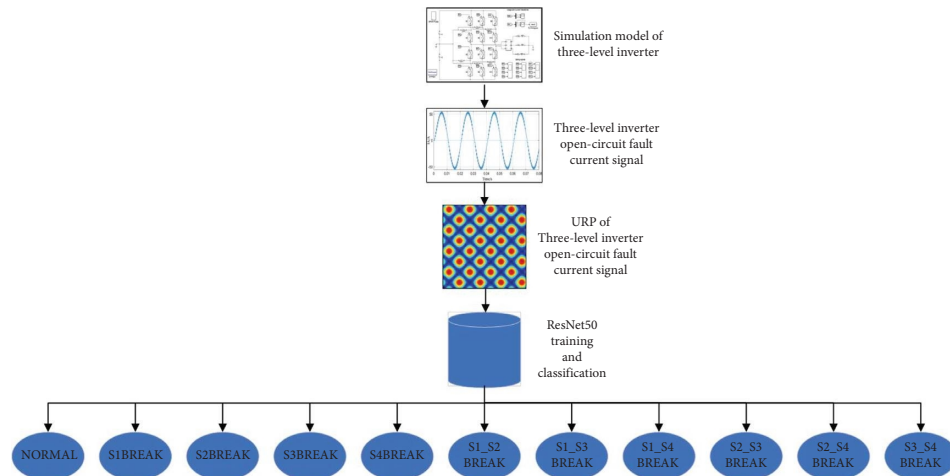


FIGURE 1: The overall process of the open-circuit fault diagnosis method in three-level inverters.

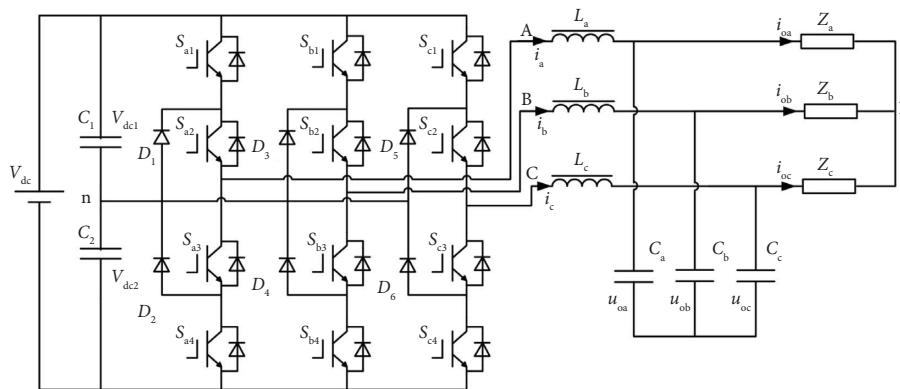


FIGURE 2: Schematic diagram of a three-level inverter.

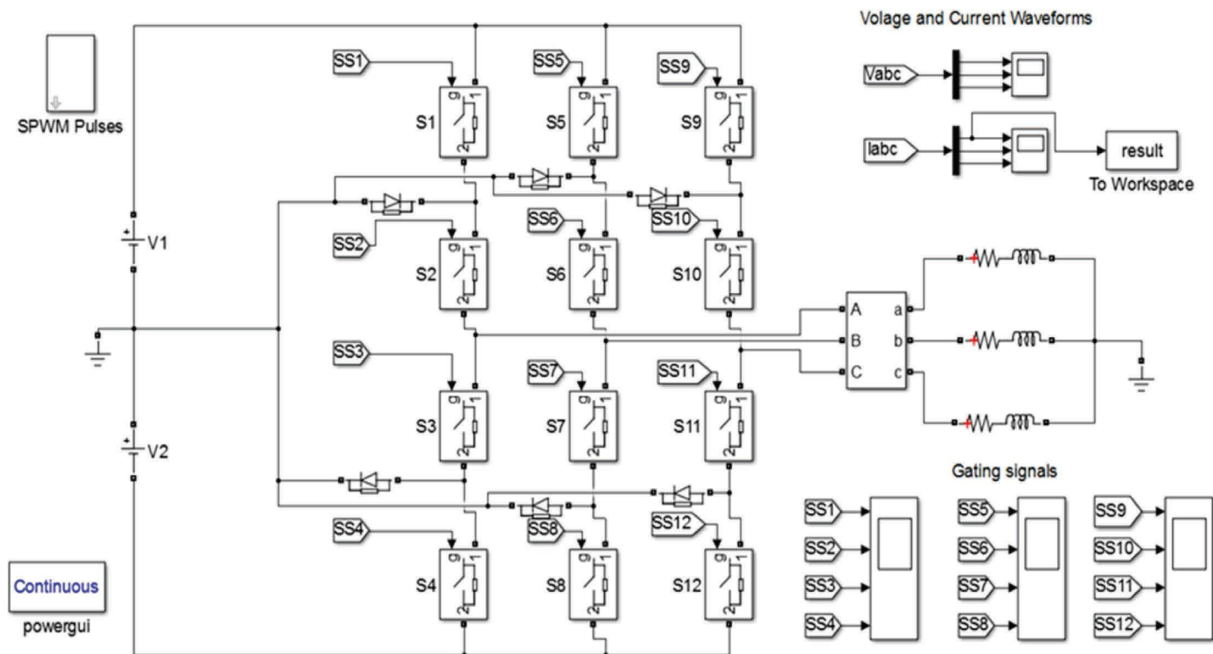


FIGURE 3: Simulation model of a three-level inverter.

TABLE 1: Classification of the IGBT open-circuit fault of a three-level inverter.

Type	Fault type	Fault location
1	IGBT operates normally without fault	None
2	Only one IGBT fails	S1, S2, S3, S4, S5, S6, S7, S8, S9, S10, S11, S12
3	Two IGBTs of different half bridges of the same bridge arm fail simultaneously	S1S3, S1S4, S2S3, S2S4, S5S7, S5S8, S6S7, S6S8, S9S11, S9S12, S10S11, S10S12
4	Two IGBTs of the same half bridge of the same bridge arm fail simultaneously	S1S2, S3S4, S5S6, S7S8, S9S10, S11S12
5	Two IGBTs of the same half bridge with different bridge arms fail	S1S5, S1S6, S1S9, S1S10, S2S5, S2S6, S2S9, S2S10, S5S9, S5S10, S6S9, S6S10, S3S7, S3S8, S3S11, S3S12, S4S7, S4S8, S4S11, S4S12, S7S11, S7S12, S8S11, S8S12
6	Two IGBT faults of cross-connection (different bridge arms and different half bridges)	S1S7, S1S8, S1S11, S1S12, S2S7, S2S8, S2S11, S2S12, S5S3, S5S4, S5S11, S5S12, S6S3, S6S4, S6S11, S6S12, S9S3, S9S4, S9S7, S9S8, S10S3, S10S4, S10S7, S10S8

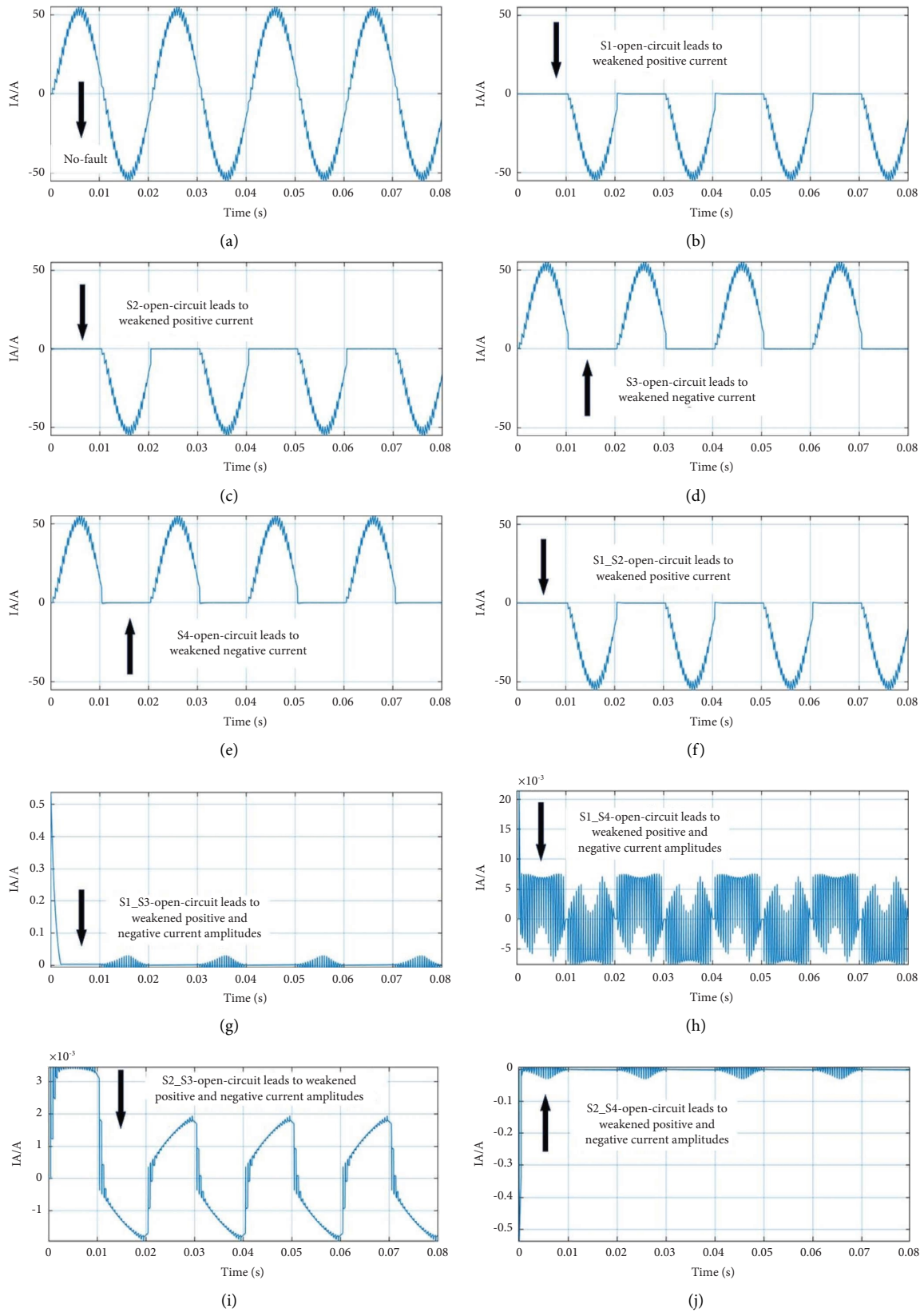


FIGURE 4: Continued.

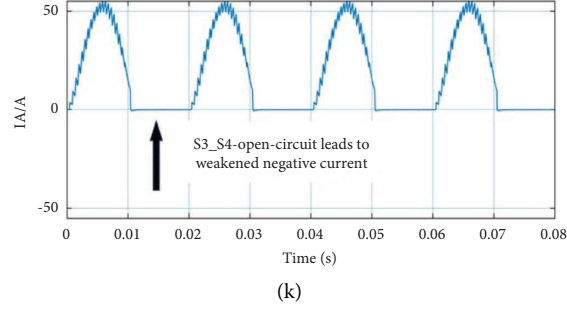


FIGURE 4: (a) No-fault current signal; (b) S1-open-circuit fault current signal; (c) S2-open-circuit fault current signal; (d) S3-open-circuit fault current signal; (e) S4-open-circuit fault current signal; (f) S1_S2-open-circuit fault current signal; (g) S1_S3-open-circuit fault current signal; (h) S1_S4-open-circuit fault current signal; (i) S2_S3-open-circuit fault current signal; (j) S2_S4-open-circuit fault current signal; (k) S3_S4-open-circuit fault current signal.

The threshold ε is a key parameter in the calculation of RPs. Unreasonable ε causes RPs to lose a large number of information features and renders them unable to reflect the dynamic characteristics of the system. Therefore, to retain the abundant nonlinear characteristics of the current signal and preserve signal details, the current signal is converted into a corresponding URPs. Figure 5 depicts the current signals for the six open-circuit faults and their URPs.

3.2. Residual NNs

3.2.1. Introduction to Residual NNs. ResNet, which is also known as a residual NN, is developed by incorporating residual learning into a traditional convolutional NN to solve the problems of gradient diffusion and accuracy decline in deep networks.

(1) Convolution Layer. Because each pixel in an image is regarded as a feature, the presence of a large number of pixel features results in extremely large weight parameters. Therefore, a convolutional NN adopts the weight sharing principle and convolution method to extract features, which can help reduce the number of weight parameters. The convolution layer is mathematically expressed as follows:

$$x_j^{(l)} = f(x_i^{(l-1)} * w_{ij}^{(l)} + b_j^{(l)}), \quad (5)$$

where $*$ represents the convolution operation, $x_j^{(l)}$ represents the output of the l th layer after the j th convolution kernel operation, $w_{ij}^{(l)}$ represents the convolution kernel, $b_j^{(l)}$ represents a biased value, and $f(\bullet)$ represents the activation function.

(2) Pool Layer. The dimension of the feature vector increases after the image is convoluted, and the calculation load of the network increases during the direct training of the network. Therefore, pooling can be used to compress the feature map and reduce the dimensions of the feature vector. Pooling can not only reduce the network's computational complexity but also maintain the number of output features. The maximum pooling layer is generally used as the downsampling layer in a convolutional NN.

(3) Average Pool Layer. In contrast to other NN models, ResNet does not contain a full connection layer. Instead, it contains a global average pooling layer, which can help reduce the number of parameters. After the average pooling layer learns the specified classification target by perceiving the global information, it yields the final classification result.

3.2.2. ResNet50. The ResNet50 network contains 49 convolutional layers and one fully connected layer and has a residual network structure that can be deeply stacked. Thus, the training process of the NN can be accelerated, and the accuracy of the model and the final classification result can be considerably improved. Figure 6 depicts the structure of a ResNet50 network.

In the residual network structure, an identity map is added using shortcut connections. The input x is directly passed to the output as the initial result, and the output result is $H(x) = F(x) + x$. When $F(x) = 0$, $H(x) = x$, which is referred to as identity mapping. Thus, using ResNet is equivalent to changing the learning target, that is, no longer learning a complete output but rather learning the difference between the target value $H(x)$ and x , which is the so-called residual $F(x)$ ($F(x) = H(x) - x$). Therefore, the subsequent training goal is to approximate the residual result to 0 so that the accuracy does not decrease as the network becomes deeper.

Figure 7 depicts the diagrams of the ResNet34 and ResNet50 NN models, whose main purpose is to reduce the number of parameters. As displayed in Figure 7(a), ResNet34 involves two $3 \times 3 \times 256$ convolutions and contains $3 \times 3 \times 256 \times 256 \times 2 = 1,179,648$ parameters. As depicted in Figure 7(b), the first 1×1 convolution in ResNet50 reduces the 256-dimensional channel to a 64-dimensional one and is finally recovered by 1×1 convolution. The total number of parameters used in ResNet50 is $1 \times 1 \times 256 \times 64 + 3 \times 3 \times 64 \times 64 + 1 \times 1 \times 64 \times 256 = 69,632$. The number of parameters in Figure 7(b) is 16.94 times that in Figure 7(a). Thus, ResNet50 reduces the number of parameters and thus the amount of computation.

As shown in Figure 8, the ResNet50 convolutional NN is a deep NN with a convolutional structure. This network is primarily composed of a convolution layer, a pooling layer,

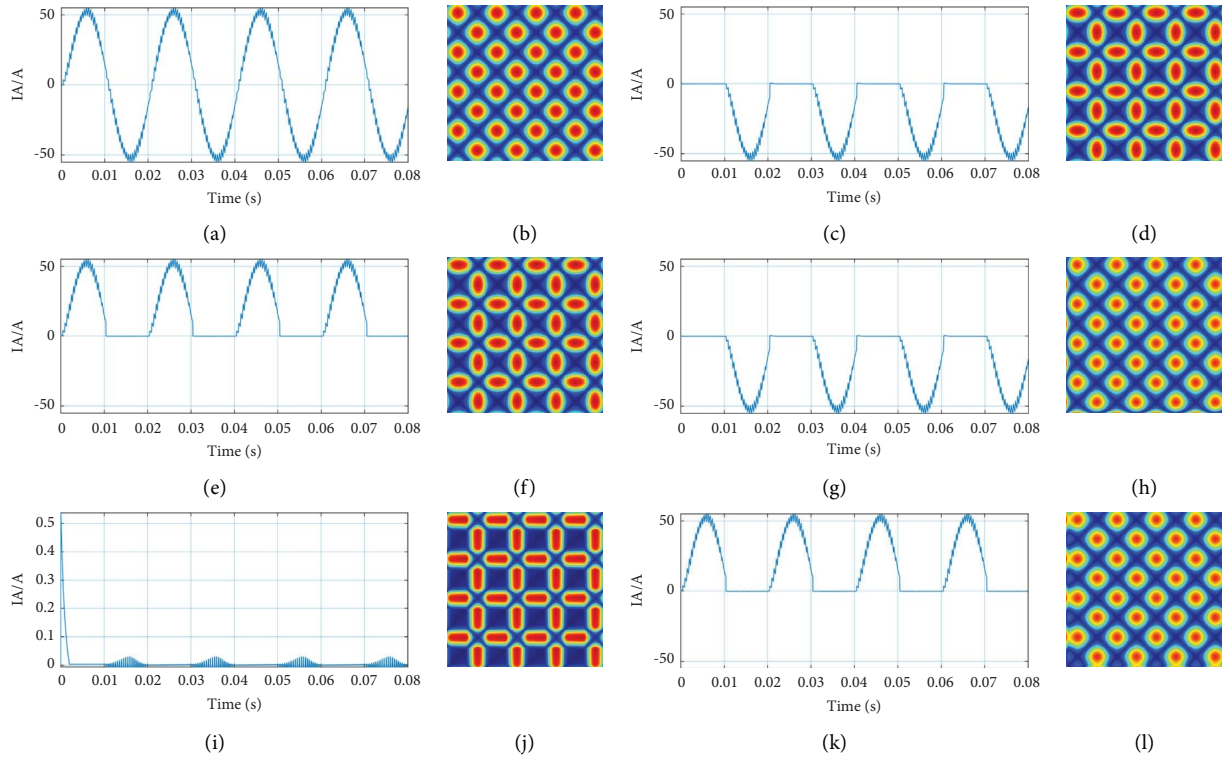


FIGURE 5: URP of the current signal and current signal. (a) No-fault current signal. (b) URP of the no-fault current signal. (c) S1-open-circuit fault current signal. (d) URP of S1-open-circuit fault current signal. (e) S3-open-circuit fault current signal. (f) URP of S3-open-circuit fault current signal. (g) S1_S2-open-circuit fault current signal. (h) URP of S1_S2-open-circuit fault current signal. (i) S1_S3-open-circuit fault current signal. (j) URP of S1_S3-open-circuit fault current signal. (k) S3_S4-open-circuit fault current signal. (l) URP of S3_S4-open-circuit fault current signal.

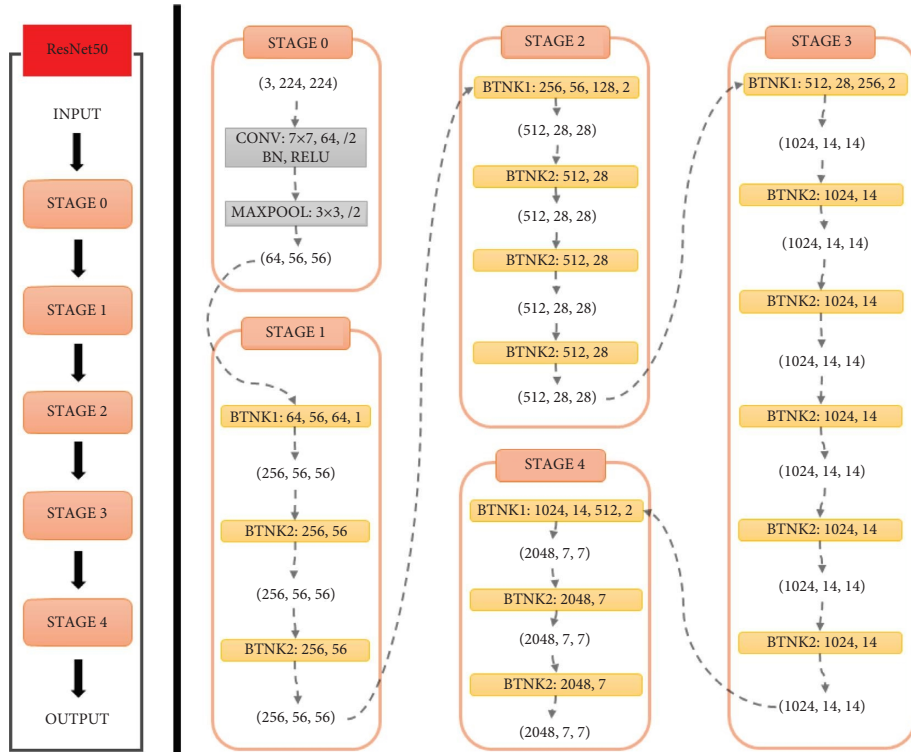


FIGURE 6: Network architecture diagram of ResNet50.

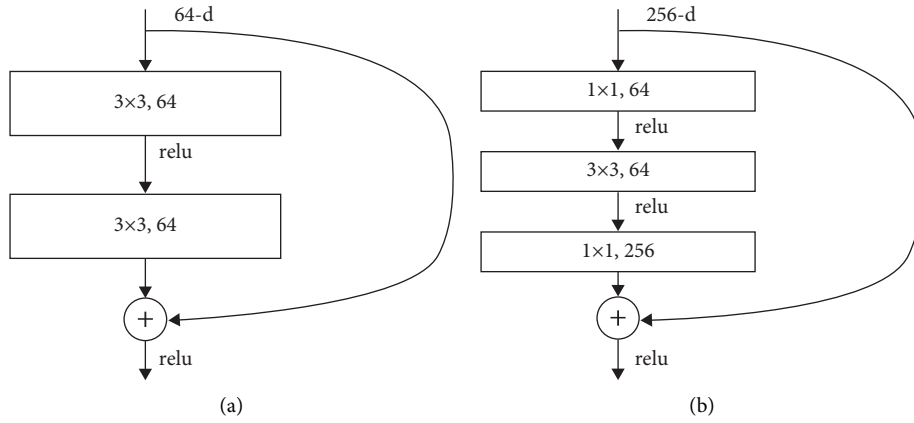


FIGURE 7: Diagram of ResNet34 and ResNet50 neural networks: (a) ResNet34; (b) ResNet50.

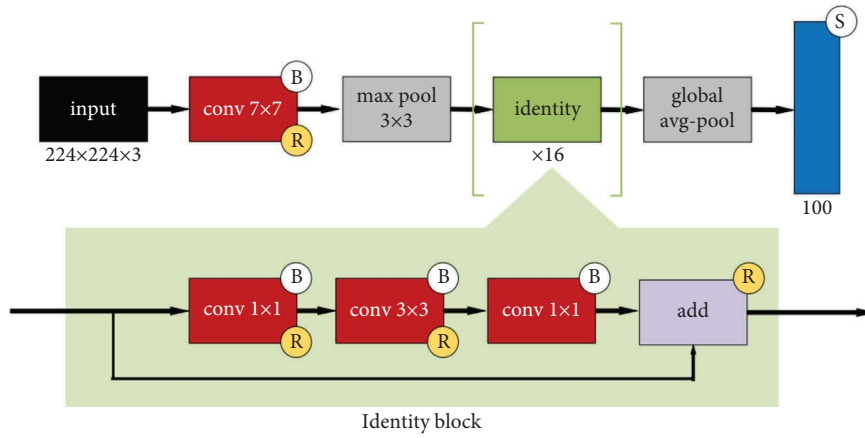


FIGURE 8: Structure diagram of the ResNet50 neural network model.

and an average pooling layer. This network has a wide range of applications in image recognition and image segmentation.

4. Experiment

4.1. Experimental Data and Processing. In deep learning, a sufficient number of samples are usually required. The higher the number of samples, the more favourable the training model effect and the stronger the model generalisation ability. During the training of the classification model, the sample input is usually taken as the amplitude of the data. When an open-circuit fault occurs in a three-level inverter, the waveform of the current signal exhibits large and regular amplitude fluctuations. The simulation data used in this study comprised 200 sets of open-circuit fault current waveforms in each category. In total, 2,200 sets of open-circuit fault current waveforms belonging to 11 categories were adopted (1,650 sets used as training sets and 550 sets used as test sets).

4.2. Experimental Results and Analysis. During the conducting of the experiment, the current waveform belonging to this type of open-circuit fault was considered the positive type, whereas the current waveform not belonging to this type of open-circuit fault was considered the negative type. Sensitivity

(SE), specificity (SP), accuracy (ACC), receiver operating characteristic (ROC) curve, and area under the ROC curve (AUC) were used to evaluate the classification model.

An ROC curve is a graphical method used to evaluate the modelling effect of binary classification models. Assuming that dichotomy is composed of positive and negative examples, the correspondence between the observed true value of dichotomy and the predicted value of the applied model is represented by a binary contingency table called the confusion matrix.

A confusion matrix is a situation analysis table in machine learning that summarises the predicted results of a classification model in the form of a matrix that aggregates the records in the dataset according to two criteria: the true category and the category judgement predicted by the classification model. Table 2 creates a dichotomous confusion matrix.

The definitions of SE, SP, and ACC are as follows:

$$\begin{aligned}
 SE &= \frac{TP}{TP + FN}, \\
 SP &= \frac{TN}{TN + FP}, \\
 ACC &= \frac{TP + TN}{TP + FP + TN + FN}.
 \end{aligned} \tag{6}$$

TABLE 2: Confusion matrix.

Actual value	Predictive value	
	Positive example	Counter example
Positive example	TP	FN
Counter example	FP	TN

According to the definition of the confusion matrix, TP represents the number of correctly predicted positive samples, FN represents the number of incorrectly classified negative samples, TN represents the number of correctly predicted negative samples, and FP represents the number of incorrectly classified positive samples.

The ordinate of an ROC curve is defined as the true positive ratio (TPR), which is also called SE and represents the proportion of samples that have been correctly classified. The horizontal coordinate of an ROC curve is defined as the false positive ratio (FPR), which represents the proportion of incorrect classifications. FPR and specific TNR are complementary; that is, the following equation is valid:

$$\begin{aligned} \text{FPR} &= 1 - \text{TNF} \\ &= 1 - \frac{\text{TN}}{\text{FP} + \text{TN}}, \end{aligned} \quad (7)$$

where FPR is usually expressed as $1 - \text{specificity}$ and SP represents specificity:

$$\text{FPR} = \frac{\text{FP}}{\text{FP} + \text{TN}}. \quad (8)$$

The ROC curve describes the relative change of the FPR and TPR. AUC describes the classification effect reflected in the ROC curve and can be used for quantitatively determining model performance. When the ROC curve cannot intuitively demonstrate the difference in classification performance between different models, it can be combined with AUC.

During the experiment, the URPs of various open-circuit faults were used as the input of ResNet50, and feature maps automatically extracted by convolutional NNs were obtained. As shown in Figure 9, the open-circuit fault current signal of the three-level inverter was converted into a URP. After the URP was processed through activation_1 of the convolution layer, various convolution kernels were used to extract different features, primarily the main texture features. The feature map output by activation_6 of the convolution layer reflected more texture details than did the feature map output by activation_1; thus, increased separability was achieved in the URPs of different types of current signals. Consequently, by setting and superimposing the convolution kernel, feature maps of texture structures of different levels were obtained. When additional convolution kernels were processed, the texture information of the RP became more comprehensive, allowing it to more fully express the nonlinear dynamic characteristics of the current signal.

To validate the URP, it was compared with the RP. According to the rule of thumb, the threshold ε was selected to be 10% of the maximum diameter of the phase space. The input training model of ResNet50 adopted a recurrence plot and no-threshold recurrence plot. The distribution of positive and negative samples in the dataset is illustrated in Table 3, the classification results are shown in Figure 10, and Figure 11 depicts the relevant ROC curves.

When the URP was used as input, favorable classification results were obtained with improved SE, SP, and ACC compared to those obtained with the RP. When combined with the ROC curve, both the URP and RP classification models yielded favorable results, with the AUC value of the URP model combined with ResNet50 being marginally higher than that of the RP model. In summary, the URP retained more detailed features than the RP, and ResNet50 yielded improved classification accuracy.

To further confirm the effectiveness of the proposed URP + ResNet50 model for inverter open-circuit fault diagnosis, we conducted a comparative study with current commonly used classification algorithms, including wavelet packet decomposition (WPD) methods such as WPD + SVM, WPD + bagging, and URP + ResNet34. The performance of different models is shown in Table 4. The corresponding bar graphs are shown in Figure 12, and the confusion matrices of URP + ResNet50 WPD + SVM, WPD + bagging, and URP + ResNet34 are shown in Figures 13–16, respectively.

As presented in Figure 12, URP + ResNet50 had the highest classification accuracy among the four methods, achieving 94.63%. On the other hand, WPD + SVM had the lowest SE and SP with values of 78.69% and 80.37%, respectively. In contrast, URP + ResNet50 had the highest SE and SP, achieving 93.35% and 95.72%, respectively, followed by URP + ResNet34 with 89.16% and 91.58%, respectively. Figure 13 shows that URP + ResNet50 identified various current fault signals of three-level inverters with an accuracy of over 90%. The ROC curve of the proposed method was superior to those of the other classification models, as shown in Figure 17, and the AUC value reached 0.9461, which was 4.42%, 14.49%, and 14.79% higher than that of the other three methods, respectively.

URP + ResNet50 achieved the highest recognition rate for 11 types of open-circuit fault current signals. In comparison with the other three methods, URP + ResNet50 achieved the best classification effect. Compared with URP + ResNet34, the recognition rates for various open-circuit fault current signals of URP + ResNet50 were improved by 4.36%, 4.12%, 4.04%, 4.53%, 4.01%, 3.73%, 5.27%, 4.19%, 4.08%, 6.19%, and 7.48%, respectively. Open-circuit faults S2_S4 and S3_S4 exhibited the highest recognition rate, leading to a significant reduction in the recognition error rate of these two types of faults. As shown in Figure 12, in the open-circuit fault diagnosis of three-stage inverters, the ResNet50 achieved an average accuracy rate of 15.39% and 13.27% higher than that of the SVM and bagging algorithms, respectively, leading to significant improvements in the recognition rate of various faults.

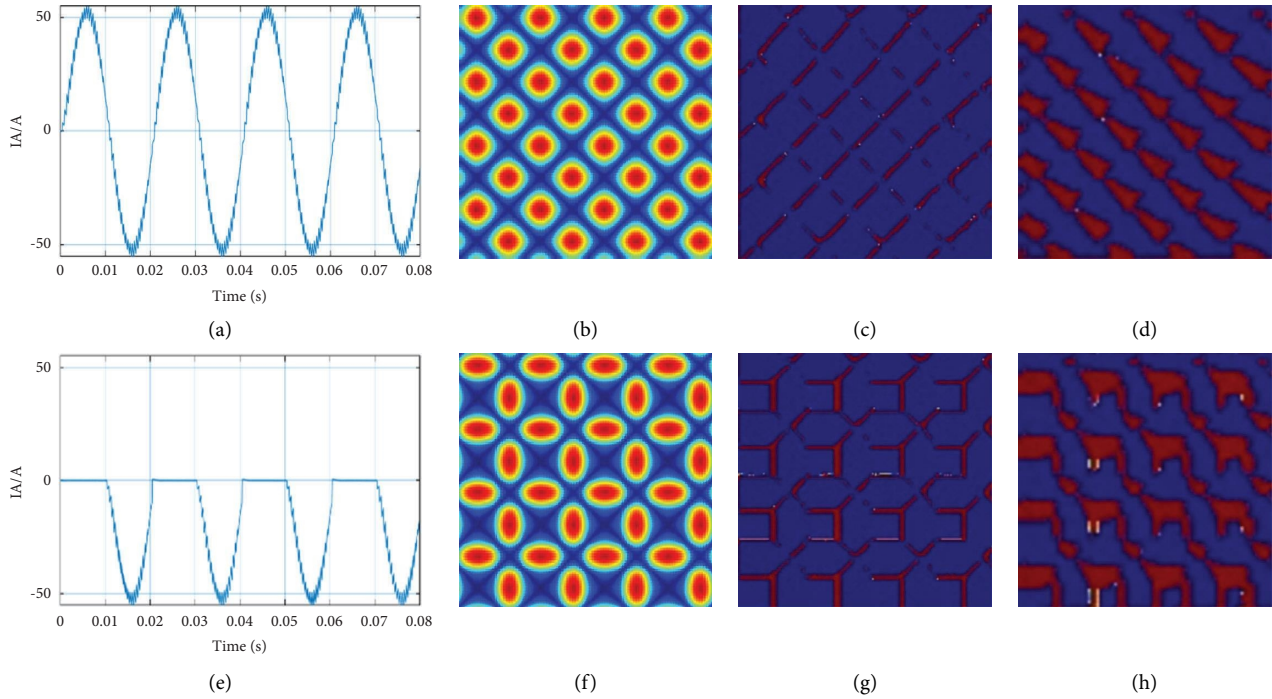


FIGURE 9: Feature extraction results of different convolution of two current signal of URP. (a) No-fault current signal. (b) URP of no-fault current signal. (c) Activation_1 of the convolutional layer. (d) Activation_6 of the convolutional layer. (e) S1-open-circuit fault current signal. (f) URP of S1-open-circuit fault current signal. (g) Activation_1 of the convolutional layer. (h) Activation_6 of the convolutional layer.

TABLE 3: Performance of two classification models.

Classification models	TP	FN	FP	TN
RP + ResNet50	1240	119	53	788
URP + ResNet50	981	69	49	1101

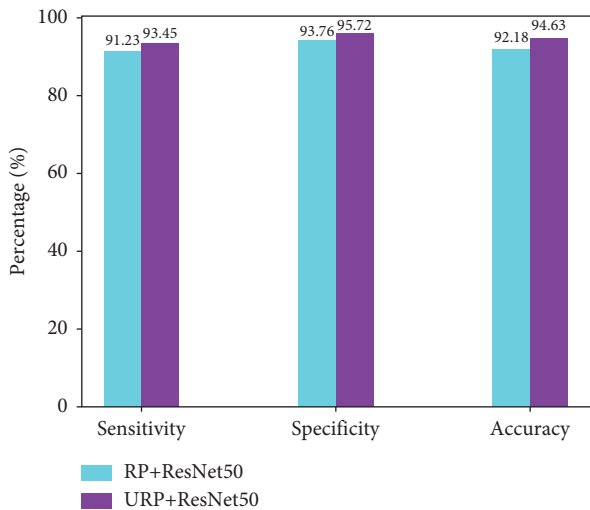


FIGURE 10: Classification results of different inputs.

4.3. Comparison of Different Diagnosis Methods.

Comparative experiments were conducted using different models, including FFT + NN and WPD + NN [33, 34]. The performance of different diagnosis methods is shown in Table 5, and the corresponding bar graphs are shown in

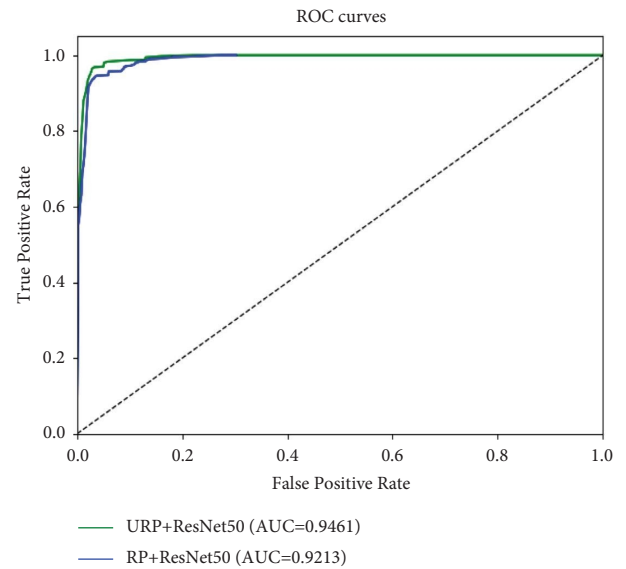


FIGURE 11: ROC curves based on different inputs of the ResNet50 model.

TABLE 4: Performance of different classification models.

Classification models	TP	FN	FP	TN
WPD + SVM	1178	319	138	565
WPD + bagging	876	216	194	914
URP + ResNet34	1170	142	75	813
URP + ResNet50	981	69	49	1101

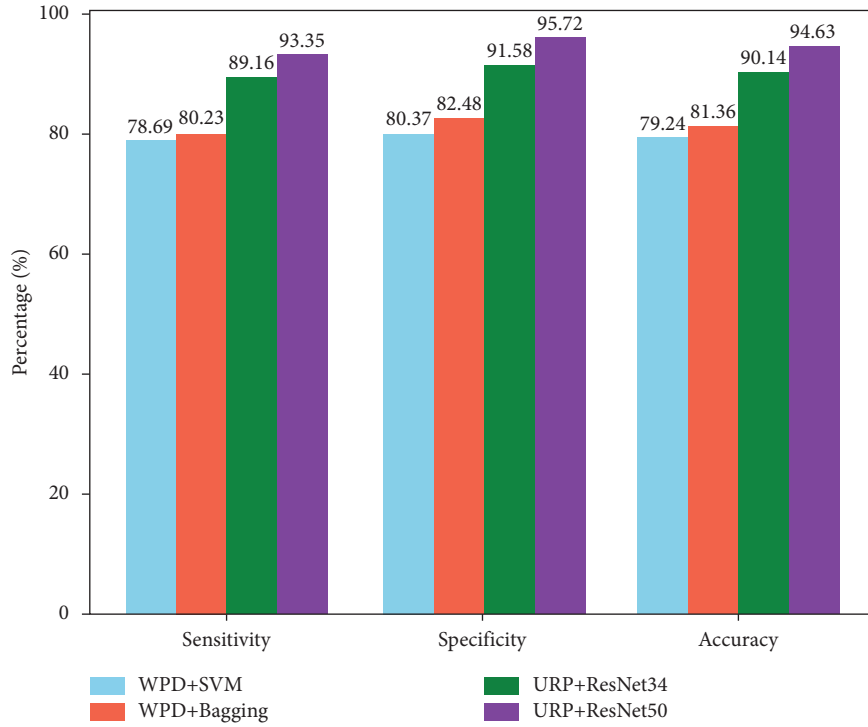


FIGURE 12: Classification results of open-circuit fault current signals.

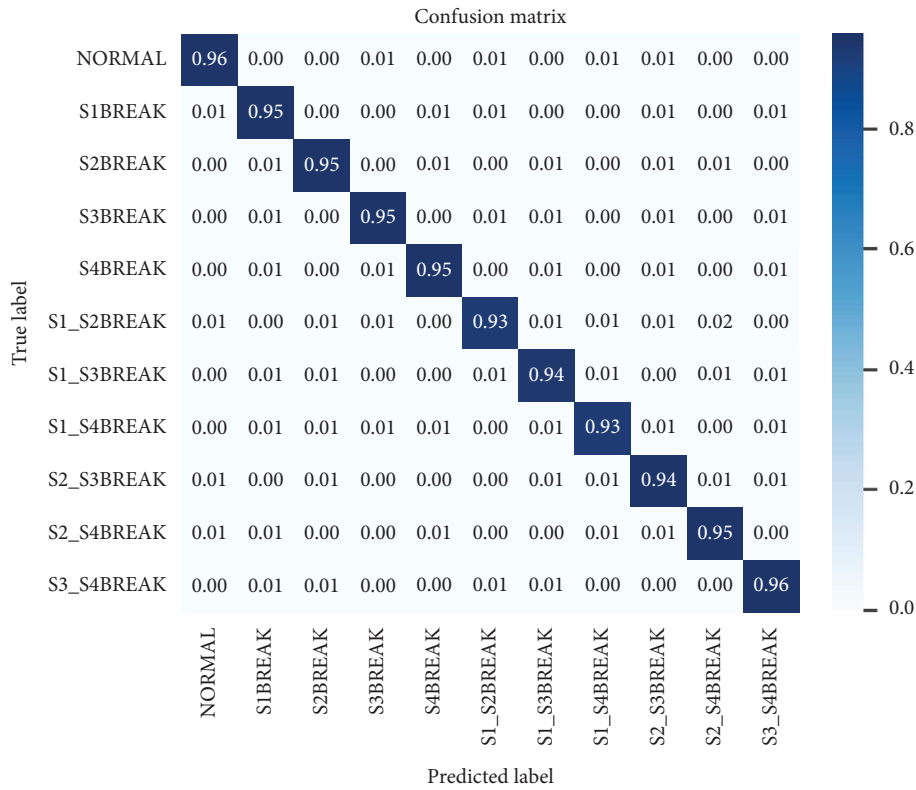


FIGURE 13: Confusion matrix of URP + ResNet50.

Figure 18. The comparison results indicated that the proposed algorithm had the highest performance in the fault diagnosis of three-level NPC inverters.

In [33], by obtaining fault characteristic values containing fault information, the time-domain signal was transformed into a frequency-domain signal through FFT,

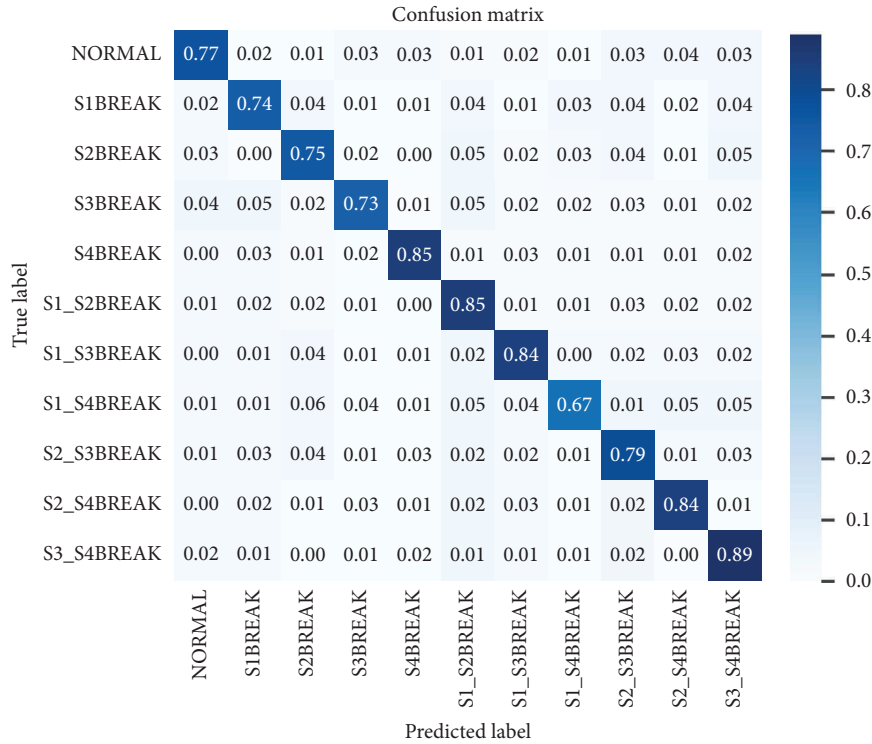


FIGURE 14: Confusion matrix of WPD + SVM.

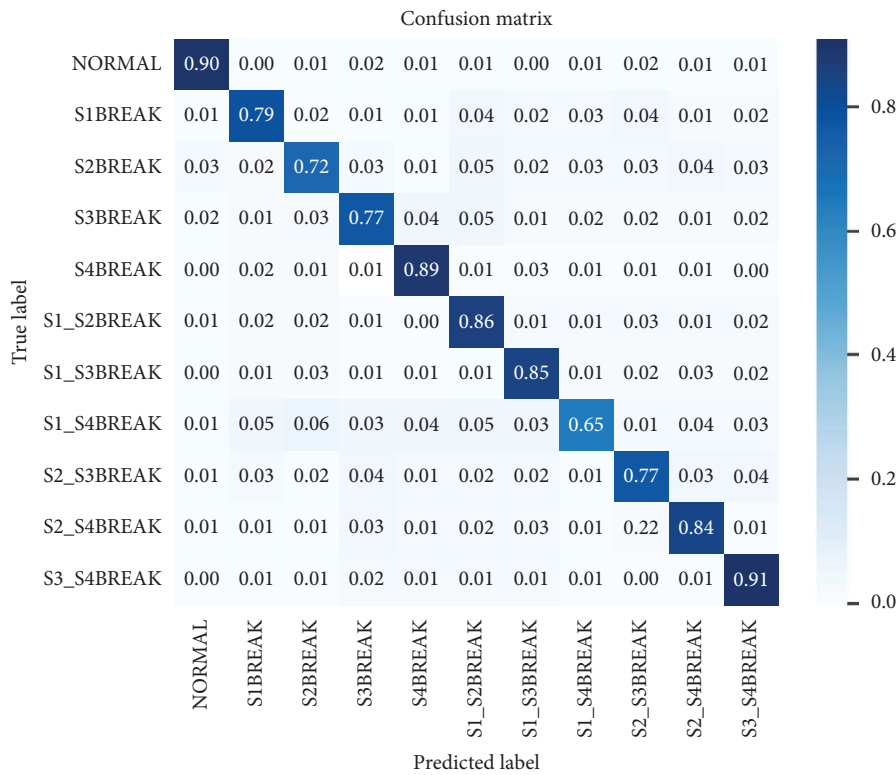


FIGURE 15: Confusion matrix of WPD + bagging.

and the correspondence between the open-circuit fault and characteristic values was then established using an NN. In [34], from the frequency-domain perspective, a wavelet

packet analysis method was used to decompose the inverter current signal in the mutually independent frequency band, and the energy values in each frequency band were then

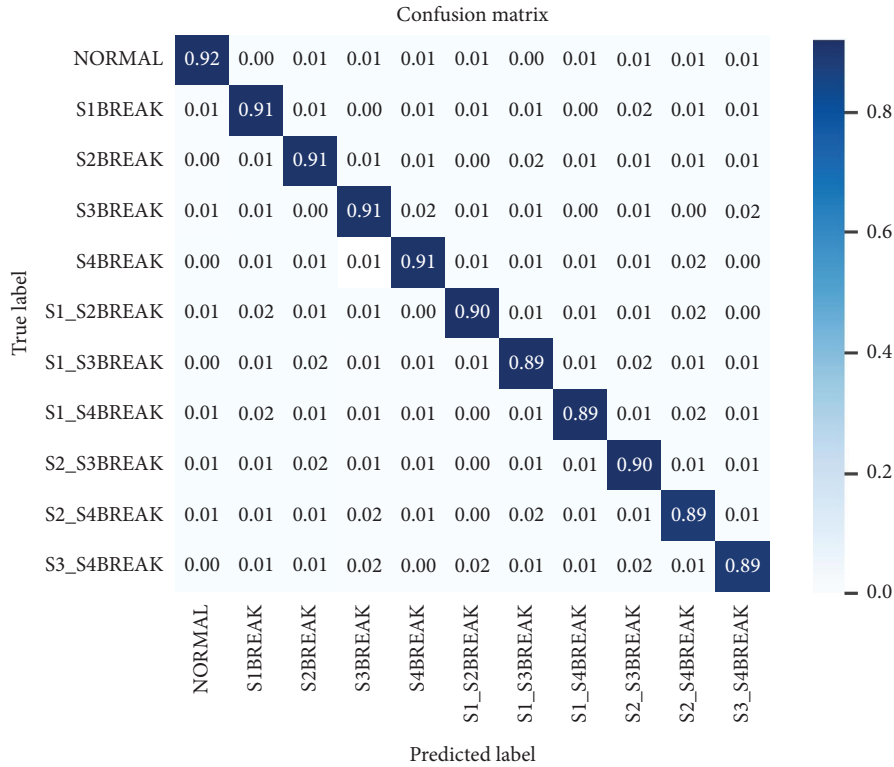


FIGURE 16: Confusion matrix of URP + ResNet34.

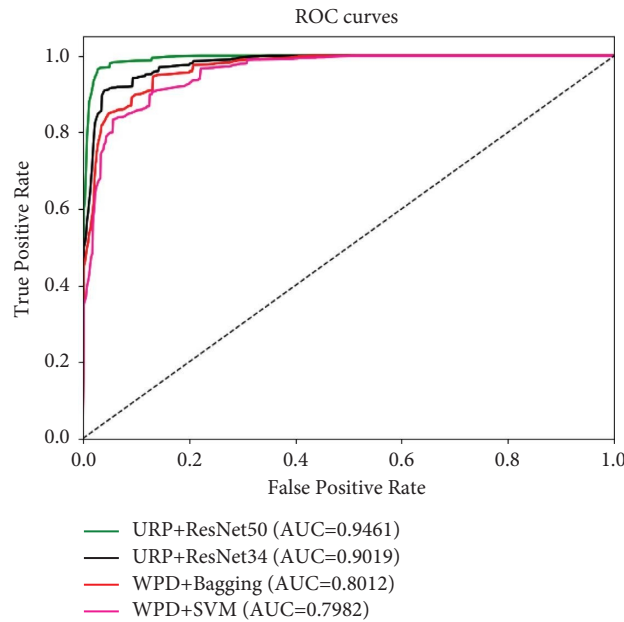


FIGURE 17: ROC curves of different methods.

formed into a vector. Subsequently, different faults corresponding to various vector values were input into an NN input unit as a feature vector. Finally, by adjusting the weight of each neural unit, a wavelet NN model was established.

The aforementioned two methods can be used to convert the current signal into a frequency-domain signal, extract the characteristic parameters of the frequency-domain, and

establish an open-circuit fault recognition NN model for three-level inverters. However, the frequency-domain analysis method cannot uncover the nonlinear information of the current signal and inevitably loses some nonlinear features. RPs are an effective means for analysing the nonlinear features of signals. Compared with other nonlinear methods, RPs do not have strict requirements

TABLE 5: Performance of different methods.

Diagnosis methods	TP	FN	FP	TN
FFT + NN	1178	319	138	565
WPD + NN	876	216	194	914
URP + ResNet50	981	69	49	1101

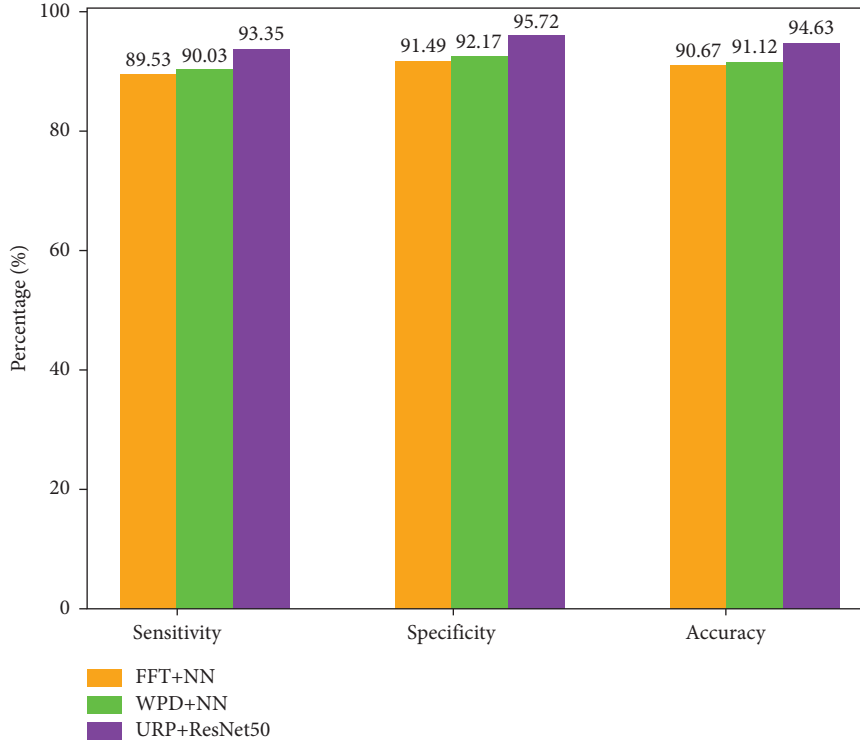


FIGURE 18: Classification results of fault identification for different methods.

regarding signal length and steadiness. Instead, the value of the threshold is used to judge the recursive point. If the threshold is selected and disregarded, a large number of detailed features are lost. However, because the URP is not restricted by a threshold, additional nonlinear information can be retained. In addition, the NN is input in the form of a one-dimensional vector, and the convolutional NN is input in the form of two-dimensional matrix data. Each network layer processes data in the form of a two-dimensional array. This form is strictly in line with the two-dimensional matrix format of digital images. An image input with a two-dimensional matrix preserves the relative position information between each pixel, which allows the network to obtain additional useful features from the input image. Therefore, the proposed method is suitable for the open-circuit fault diagnosis of three-level inverters.

In summary, by converting the current signals of different open-circuit faults in three-level inverters into URPs, the nonlinear features of the signals were accurately mapped to a two-dimensional plane, and additional nonlinear information of the current signals was retained. The URPs of the current signals were then input into ResNet50 for training, and classification models of different open-circuit faults were established. On the basis of traditional convolutional NNs,

ResNet50 uses residual learning framework to solve the problems of gradient dispersion and precision decline in deep networks, which facilitates the training process and improves the model's generalisation ability. Consequently, additional detailed features can be learned from URPs, and favourable classification results can be obtained.

5. Conclusions

In this study, open-circuit faults of IGBTs in three-level NPC inverters were investigated. A new fault diagnosis system comprising URPs and convolutional NNs was developed. The original fault signal was obtained by adopting an inverter model constructed using the Simulink module of MATLAB. The current fault signal was then converted into a URP by using nonlinear dynamics, and its nonlinear features were then mapped to a two-dimensional plane. Subsequently, feature self-learning and training of the URP were performed by a ResNet50 residual NN to obtain a current signal classification model. The experimental results indicated that the proposed method exhibited strong fault diagnostic capability, with a diagnostic accuracy rate of 94.61%, a sensitivity rate of 93.35%, and a specificity rate of 95.72%.

In this study, URPs and ResNet50 were combined and used for fault signal generation, signal conversion, and fault identification. The experimental results indicated that compared with other fault classification models, the proposed fault diagnosis model (URP + ResNet50 model) had higher fault identification accuracy. Moreover, the proposed model exhibited strong adaptability. Thus, the proposed model can be used in the open-circuit fault diagnosis of three-level inverters. Future studies should focus on improving the diagnostic accuracy of this model and discovering additional fault patterns and features.

Data Availability

The datasets generated and analysed during the current study are not publicly available due to the confidentiality of the data but are available from the corresponding author on reasonable request.

Conflicts of Interest

The authors declare that they have no conflicts of interest.

Acknowledgments

This work was supported by the Shanghai Science and Technology Committee Funding (No. 17DZ1201201).

References

- [1] G. Nageswara Rao, P. Sangameswara Raju, and K. Chandra Sekhar, "Harmonic elimination of cascaded H-bridge multilevel inverter based active power filter controlled by intelligent techniques," *International Journal of Electrical Power and Energy Systems*, vol. 61, pp. 56–63, 2014.
- [2] B. Fan, Z. Cao, and C. Wang, "A novel neutral-point potential balance control method based on voltage feedback for neutral-point clamped three-level inverter," *International Journal of Electrical Power & Energy Systems*, vol. 145, Article ID 108583, 2023.
- [3] M. Humayun, M. M. Khan, and M. U. Hassan, "Analysis of hybrid switches symmetric flying capacitor multilevel inverter based STATCOM," *International Journal of Electrical Power & Energy Systems*, vol. 131, Article ID 107054, 2021.
- [4] H. Katir, A. Abouloifa, and K. Noussi, "PV-powered grid-tied fault tolerant double-stage DC-AC conversion chain based on a cascaded H-bridge multilevel inverter," *IFAC-PapersOn-Line*, vol. 55, no. 12, pp. 103–108, 2022.
- [5] V. Smet, F. Forest, and J. J. Huselstein, "Ageing and failure modes of IGBT modules in high-temperature power cycling," *IEEE Transactions on Industrial Electronics*, vol. 58, no. 10, pp. 4931–4941, 2011.
- [6] Y. Yu and S. Pei, "Open-circuit fault diagnosis of neutral point clamped three-level inverter based on sparse representation," *IEEE Access*, vol. 6, pp. 73499–73508, 2018.
- [7] Z. Chen, Z. Yu, and X. Zhang, "Analysis and experiments for IGBT, IEGT, and IGCT in hybrid DC circuit breaker," *IEEE Transactions on Industrial Electronics*, vol. 65, no. 4, pp. 2883–2892, 2018.
- [8] J. Liang, K. Zhang, and A. Al-Durra, "A state-of-the-art review on wind power converter fault diagnosis," *Energy Reports*, vol. 8, pp. 5341–5369, 2022.
- [9] R. Bolbolnia, K. Abbaszadeh, and M. Nasiri, "Diagnosis and fault-tolerant control of six-phase wind turbine under multiple open-switch faults," *Mathematical Problems in Engineering*, vol. 2021, Article ID 9999918, 16 pages, 2021.
- [10] S. M. Kim, J. S. Lee, and K. B. Lee, "A modified level-shifted PWM strategy for fault-tolerant cascaded multilevel inverters with improved power distribution," *IEEE Transactions on Industrial Electronics*, vol. 63, no. 11, pp. 7264–7274, 2016.
- [11] H. Yan, Y. Xu, and J. Zou, "A novel open-circuit fault diagnosis method for voltage source inverters with a single current sensor," *IEEE Transactions on Power Electronics*, vol. 33, no. 10, pp. 8775–8786, 2018.
- [12] Z. Wang, Z. Huang, and C. Song, "Multiscale adaptive fault diagnosis based on signal symmetry reconstitution pre-processing for microgrid inverter under changing load condition," *IEEE Transactions on Smart Grid*, vol. 9, no. 2, pp. 797–806, 2018.
- [13] P. Mehta, S. Sahoo, and H. Dhiman, "Open circuit fault diagnosis in five-level cascaded H-bridge inverter," *International Transactions on Electrical Energy Systems*, vol. 2022, Article ID 8588215, 13 pages, 2022.
- [14] L. M. A. Caseiro and A. M. S. Mendes, "Real-time IGBT open-circuit fault diagnosis in three-level neutral-point-clamped-voltage-source rectifiers based on instant voltage error," *IEEE Transactions on Industrial Electronics*, vol. 62, no. 3, pp. 1669–1678, 2015.
- [15] C. Shu, C. Ya-Ting, and Y. Tian-Jian, "A novel diagnostic technique for open-circuited faults of inverters based on output line-to-line voltage model," *IEEE Transactions on Industrial Electronics*, vol. 63, no. 7, pp. 4412–4421, 2016.
- [16] A. M. S. Mendes, M. B. Abadi, and S. M. A. Cruz, "Fault diagnostic algorithm for three-level neutral point clamped AC motor drives, based on the average current Park's vector," *IET Power Electronics*, vol. 7, no. 5, pp. 1127–1137, 2014.
- [17] A. Joseph, T. R. Chelliah, and R. Selvaraj, "Fault diagnosis and fault-tolerant control of megawatt power electronic converter-fed large-rated asynchronous hydrogenerator," *IEEE Journal of Emerging and Selected Topics in Power Electronics*, vol. 7, no. 4, pp. 2403–2416, 2019.
- [18] I. Jlassi and A. J. M. Cardoso, "IGBTs and current sensors fault diagnosis in direct-drive PSMG wind turbine systems using adaptive thresholds," in *Proceedings of the IECON 2017-43rd Annual Conference of the IEEE Industrial Electronics Society*, pp. 5072–5077, Beijing, China, October 2017.
- [19] J. O. Estima and A. J. Marques Cardoso, "A new algorithm for real-time multiple open-circuit fault diagnosis in voltage-fed PWM motor drives by the reference current errors," *IEEE Transactions on Industrial Electronics*, vol. 60, no. 8, pp. 3496–3505, 2013.
- [20] T. Yang, H. Pen, and Z. Wang, "Feature knowledge based fault detection of induction motors through the analysis of stator current data," *IEEE Transactions on Instrumentation and Measurement*, vol. 65, no. 3, pp. 549–558, 2016.
- [21] W. J. Kim and S. H. Kim, "ANN design of multiple open-switch fault diagnosis for three-phase PWM converters," *IET Power Electronics*, vol. 13, no. 19, pp. 4490–4497, 2020.
- [22] W. Rongjie, Z. Yiju, and Z. Haifeng, "A fault diagnosis method for three-phase rectifiers," *International Journal of Electrical Power & Energy Systems*, vol. 52, pp. 266–269, 2013.
- [23] Z. Huang, Z. Wang, and H. Zhang, "A diagnosis algorithm for multiple open-circuited faults of microgrid inverters based on main fault component analysis," *IEEE Transactions on Energy Conversion*, vol. 33, no. 3, pp. 925–937, 2018.

- [24] W. Gong, H. Chen, and Z. Zhang, "A data-driven-based fault diagnosis approach for electrical power DC-DC inverter by using modified convolutional neural network with global average pooling and 2-D feature image," *IEEE Access*, vol. 8, pp. 73677–73697, 2020.
- [25] M. Fei, L. Ning, and M. Huiyu, "On-line fault diagnosis model for locomotive traction inverter based on wavelet transform and support vector machine," *Microelectronics Reliability*, vol. 88-90, pp. 1274–1280, 2018.
- [26] F. Asghar, M. Talha, and S. H. Kim, "Neural network based fault detection and diagnosis system for three-phase inverter in variable speed drive with induction motor," *Journal of Control Science and Engineering*, vol. 2016, Article ID 1286318, 12 pages, 2016.
- [27] B. D. E. Cherif and A. Bendiabdellah, "Detection of two-level inverter open-circuit fault using a combined DWT-NN approach," *Journal of Control Science and Engineering*, vol. 2018, Article ID 1976836, 11 pages, 2018.
- [28] T. Wang, J. Qi, and H. Xu, "Fault diagnosis method based on FFT-RPCA-SVM for cascaded-multilevel inverter," *ISA Transactions*, vol. 60, pp. 156–163, 2016.
- [29] H. Hu, F. Feng, and T. Wang, "Open-circuit fault diagnosis of NPC inverter IGBT based on independent component analysis and neural network," *Energy Reports*, vol. 6, pp. 134–143, 2020.
- [30] S. Liu, X. Qian, and H. Wan, "NPC three-level inverter open-circuit fault diagnosis based on adaptive electrical period partition and random forest," *Journal of Sensors*, vol. 2020, Article ID 9206579, 18 pages, 2020.
- [31] S. Gunther, L. Ruthotto, and J. B. Schroder, "Layer-parallel training of deep residual neural networks," *SIAM Journal on Mathematics of Data Science*, vol. 2, no. 1, pp. 1–23, 2020.
- [32] X. J. Meng, S. Qiu, and S. Wan, "A motor imagery EEG signal classification algorithm based on recurrence plot convolution neural network," *Pattern Recognition Letters*, vol. 146, pp. 134–141, 2021.
- [33] W. Jiang, C. Wang, and Y. Li, "Fault detection and remedy of multilevel inverter based on BP neural network," in *Proceedings of the Asia-Pacific Power and Energy Engineering Conference*, pp. 1–4, Xiamen, China, April 2012.
- [34] R. Hua and P. P. Ji, "Research on the NPC three-level inverter fault feature extraction method based on wavelet analysis," *Applied Mechanics and Materials*, vol. 494-495, pp. 1410–1413, 2014.